Journal of Magnetism and Magnetic Materials 517 (2021) 167388

Contents lists available at ScienceDirect

Journal of Magnetism and Magnetic Materials

journal homepage: www.elsevier.com/locate/jmmm

Research articles

Magnetisation and magnetic anisotropy of ion beam synthesised iron nitride

P. Gupta[a], H. Fiedler[a], S. Rubanov[b], J. Kennedy[a,c,*]

[a] National Isotope Centre, GNS Science, PO Box 31312, Lower Hutt 5010, New Zealand
[b] Advanced Microscopy Facility, Bio21 Institute, University of Melbourne, Victoria, 3010, Australia
[c] The MacDiarmid Institute for Advanced Materials and Nanotechnology, New Zealand

ARTICLE INFO

Keywords:
Iron nitride
Nitrogen ordered martensite
Ion implantation
Magnetic moment/magnetisation
Perpendicular magnetic anisotropy
Sputtering
Ion beam analysis
Transmission electron microscopy

ABSTRACT

We report the effects of implantation-induced-sputtering in determining the true magnetisation of iron nitrides formed by nitrogen implantation into iron films and the changes subsequently observed in their magnetic anisotropy. Iron thin films (40 nm) capped with gold layers were synthesized by ion beam sputtering. Nitrogen was implanted onto the thin film to a dose of 7×10^{16} cm^{-2}. Dynamic ion–solid interaction simulations calculate the average nitrogen concentration within the iron thin films to be 13 at.%. Ion beam analysis was used to evaluate the composition and depth profile of the thin films before and after implantation. Cross-sectional transmission electron microscopy helped in identifying the implantation induced effects at the surface and interface of the thin film structure. Magnetisation measurements show that nitrogen implantation enhances the magnetisation of thin films and reduces their in-plane magnetic anisotropy. High resolution TEM and magnetisation results suggest formation of α'/α"-$Fe_{16}N_2$ with large magnetic moments and perpendicular magnetic anisotropy. The enhancement in magnetisation of the thin film with and without considering the sputtering losses is determined to be 15% and 5%, respectively. Our review of literature shows that underestimating the sputtering losses from implantation leads to reporting of inconsistent and reduced magnetic moments for $Fe_{16}N_2$.

1. Introduction

Incorporation of light elements into iron matrix has resulted in materials with extremely useful properties and wide-ranging applications. Steel, the most widely used alloy, is one such example formed by adding carbon to iron. Nitrogen incorporation into the interstitial sites of iron leads to formation of iron nitrides with applications in diverse fields such as catalysis [1], cancer treatment [2], lightweight permanent magnets [3,4], electrochemical energy devices [5,6], corrosion and wear-resistant surfaces [7] etc. Ferromagnetic iron nitrides, in particular, are an attractive material choice for high density magnetic data storage media and read heads, magnetic sensors and motors [8–11].

α-Fe is a weak ferromagnet with partially filled 3d↑ states contributing to a magnetic moment of 2.22 μ_B at 0 K. It assumes a BCC structure with the easy axis of magnetisation oriented along the ⟨0 0 1⟩ axis [12]. Nitrogen incorporation dilates its crystal axis and switches the easy axis of magnetisation towards its c-axis leading to perpendicular magnetic anisotropy (PMA). Bonding with nitrogen also compensates the unfilled 3d states of iron leading to enhanced saturated magnetic moments [12]. There is also a considerable reduction in magnetostriction whilst retaining a high degree of spin polarisation [12]. Perpendicular magnetic anisotropy is a highly desirable property for magnetic thin film applications as they allow spin transfer torque switching at lower currents and provide thermal stability. Materials possessing PMA such as iron nitrides are proven to be useful for fabricating ultra-fast MRAM, high density data storage and voltage-controlled spintronic devices [13,14].

Iron nitrides exist in many different phases. Some of the highest magnetic moments for iron reported in literature are attributed to the formation of chemically ordered nitrogen-martensite (α"-$Fe_{16}N_2$), a metastable bct phase of iron nitride with N = 11.6 at.% [15]. However, it has been difficult to ascertain the exact magnetic moment of this iron nitride phase with several contradicting reports in literature [12,15–20]. Different synthesis approaches such as chemical vapor deposition, reactive magnetron sputtering, molecular beam epitaxy, ion implantation, ammonolysis, tempering etc., have been pursued to fabricate α"-$Fe_{16}N_2$ as thin films [3,21]. However, obtaining pure α"-$Fe_{16}N_2$ phase has been challenging. The difficulty arises from lack of control over the nitrogen concentration and distribution across the thin film whilst maintaining the metastable conditions necessary for its synthesis. Growth of α-Fe thin films followed by N implantation is reported to be an effective method in synthesizing thin films with high volume fractions of α"-$Fe_{16}N_2$ [19,22,23]. This can primarily be

* Corresponding author at: National Isotope Centre, GNS Science, PO Box 31312, Lower Hutt 5010, New Zealand.
E-mail address: j.kennedy@gns.cri.nz (J. Kennedy).

https://doi.org/10.1016/j.jmmm.2020.167388
Received 21 July 2020; Received in revised form 31 August 2020; Accepted 1 September 2020
Available online 12 September 2020
0304-8853/

attributed to two key advantages of this method – (1) ion implantation offers a non-thermal equilibrium synthesis approach that allows formation of metastable structures at ambient temperature (bulk), and (2) ion implantation technique provides precise control over dopant concentration and distribution.

Determining the true magnetic moment of iron nitride synthesized by ion implantation has proven to be challenging. This is evidenced by the wide range of values reported for the magnetisation of ion beam synthesized α"-$Fe_{16}N_2$ and a lack of consensus on their true magnetic moment [3,19,22–30]. To determine the magnetic moment of ion beam synthesized iron nitride, the change in magnetic moment of iron thin film after nitrogen implantation must be normalised against the volume fraction of nitride formed. For this approach to be successful, both the volume fraction of the nitride phase formed and the change in magnetisation of the iron thin film after implantation must be measured accurately. Use of Mossbauer spectroscopy allows precise determination of the volume fraction of iron nitride phases formed. However, measuring the change in magnetisation of iron thin film after implantation is not straight forward due to secondary effects of ion implantation.

Apart from introducing dopants into a solid matrix, ion implantation also results in sputtering, i.e., removal of atoms near the surface and intermixing of atoms within the target. Both these effects can reduce the measured magnetic moments of the sample significantly. However, most works on ferromagnetic iron nitride synthesized by implantation either ignore or underestimate these effects leading to reporting of reduced magnetic moments for the iron nitride phase. In this work, we will demonstrate the significance of considering these secondary effects in determining the true magnetic moment of N implanted iron thin films. Our work may partially resolve the differences observed in literature and would better equip future studies in achieving consistent results.

2. Methods and materials

Thin films were sputter deposited on silicon substrate using the ion beam sputtering system at GNS Science. This method allows thin film fabrication from both conducting and insulating solid targets under high vacuum conditions. Detailed information on the setup can be found in [31]. In this work, 40 nm thick Fe film followed by a 30 nm Au capping layer has been deposited into Si substrates. Nitrogen (N^+) was implanted into the Fe thin films using the low-energy ion implanter at GNS Science [32]. The system uses a Penning gas ion source and is coupled to a 90° dipole electromagnet for mass separation. Several focussing lenses are used throughout the transport column to focus the ion beam through the magnet and ultimately to the target stage in the sample chamber. The setup allows accurate control over the implantation energy and fluence [32,33]. Nitrogen was used as the precursor gas. The Penning ion source was operated with an anode voltage of 2 kV and a total terminal voltage of 30 kV. The selected energy allows a near homogeneous distribution of nitrogen within the Fe thin film. N^+ ions were selected by passing the extracted ion beams through the electromagnet (radius = 40 cm) which separates the ions based on mass, charge and velocity. The mass resolution was further improved using slits in the beam line. The process was carried out at a low base pressure of $\leq 5 \times 10^{-5}$ Pa in the sample chamber to ensure high purity. The ion beam current was limited to < 5 μA/cm^2 to minimise bulk heating effects. A charge integrator connected to the target holder measures the implantation fluence. The as-deposited thin films were implanted with a dose of 7×10^{16} N cm^{-2}. The selected dose is expected to limit the N concentration between 10 and 15 at.% within the Fe thin film.

The effects of N implantation on the sample were simulated using the dynamic ion-solid interaction code (T-DYN) software package [34–36]. T-DYN simulations, compared to the TRIM simulations that are usually employed, provide a more accurate estimate of the losses due to sputtering. This is because T-DYN calculations consider the dynamic changes in the composition of thin film during implantation which is known to play a significant role in high dose implantation. This is especially important in this study since prior studies in this area has either neglected or underestimated the sputtering induced effects on the nitrogen implanted iron films. The target is constructed of 100 cells each with an area of 10000 Å^2 and a width of 10 Å. The target is composed of three layers – Si substrate (300 Å), Fe thin film (400 Å), Au capping layer (300 Å).

Rutherford backscattering spectrometry (RBS) was used to measure the thickness and elemental composition of the as-deposited and implanted iron films [33,37]. A 2 MeV $^4He^+$ beam with 20 nA current and collimated to 1 mm in diameter was used for measurements. A surface barrier detector with 20 keV resolution was placed at an angle of 165° to the incident beam to detect the backscattered particles. The solid angle of detection of the setup was 0.54 msr. The charge collected for each measurement was set to 20 μC. Each sample was measured at multiple spots to check the uniformity of implantation and deposition. For the quantification of nitrogen implanted into the films, Nuclear Reaction Analysis (NRA) was performed with a 920 keV D^+ beam with 10–20 nA current [33]. The total charge collected for each measurement was 20 μC. The NRA detector – a surface barrier detector, was placed behind 10 μm of Mylar foil at an angle of 150° to the incident ion beam. The energy of the emitted particles is characteristic for the nuclear reactions and the yield determines the amount of the element in the sample. NRA is ideal to detect light elements on a heavy element matrix.

Cross-sectional TEM was performed on N implanted and as-deposited samples to image and identify the implantation induced effects on thin film surface and interface. The samples were prepared using lift-out technique described elsewhere [38]. The cross-sectional images were obtained using FEI Tecnai F20 transmission electron microscope operated at 200 kV. High resolution TEM images of the implanted samples were obtained to characterise any crystal structure present in the implanted sample. A magnetic property measurement system (MPMS) from Quantum Design was used to probe the magnetic properties of the as-deposited and implanted thin films. The magnetic moment of the samples was measured as a function of applied magnetic field from 0 to 5 T at 300 K. Measurements were taken with the applied field in both parallel and perpendicular direction to the sample surface plane.

3. Results and discussion

T-DYN simulations were performed to compute the effects of N^+ implantation onto Au capped Fe thin films. The elemental distribution obtained as an output of the simulation is plotted in Fig. 1.

The simulation yields several key results. First, N^+ implantation at 32 keV energy to a dose of 7×10^{16} cm^{-2} results in an average nitrogen concentration of 13 at.% across the Fe thin film. Secondly, implantation results in significant sputtering loss and surface recession (15 nm) of the capping layer. However, no significant losses in iron concentration is predicted. It is worthwhile to note that the sputter yield of 32 keV N^+ on Au and Fe is 1.3 and 1 respectively. Thirdly, the implantation causes substantial intermixing among gold and iron layers at the surface and silicon and iron layers at the substrate interface. The dashed lines in the figure represent the sharp boundary between the different layers before implantation. Substantial amount of iron is observed to have moved towards the surface after implantation. The simulation predicts the surface concentration of Au, Fe and N to be 65 at.%, 24 at.% and 11 at.% respectively.

Rutherford backscattering spectrometry was performed to analyse the changes in the elemental depth profile of the Fe thin film upon N implantation and to quantify the total Fe content in film before and after implantation. SIMNRA software was used to interpret RBS data [39]. Fig. 2 shows RBS spectra of the as-deposited and implanted films

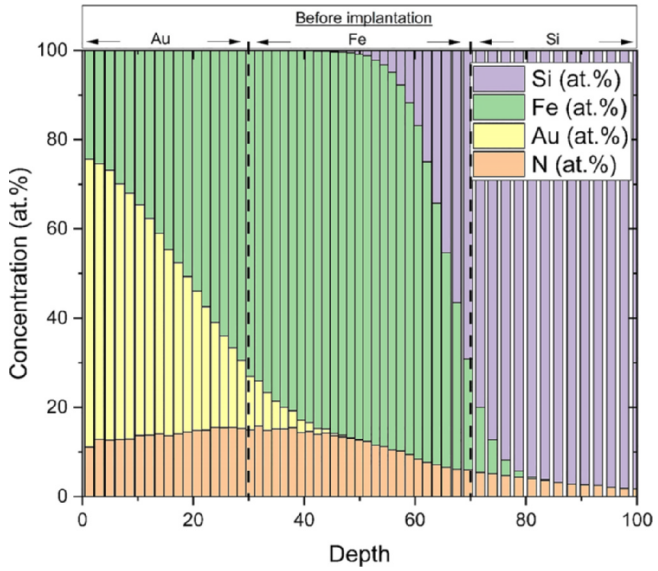

Fig. 1. T-DYN simulation output of target cell (Au 300 Å/ Fe 400 Å/Si 300 Å) implanted with 32 keV N^+ ions to a dose of 7 × 10^{16} cm^{-2}. The dashed lines represent the position of the Au/Fe and Fe/Si interfacial boundaries before implantation.

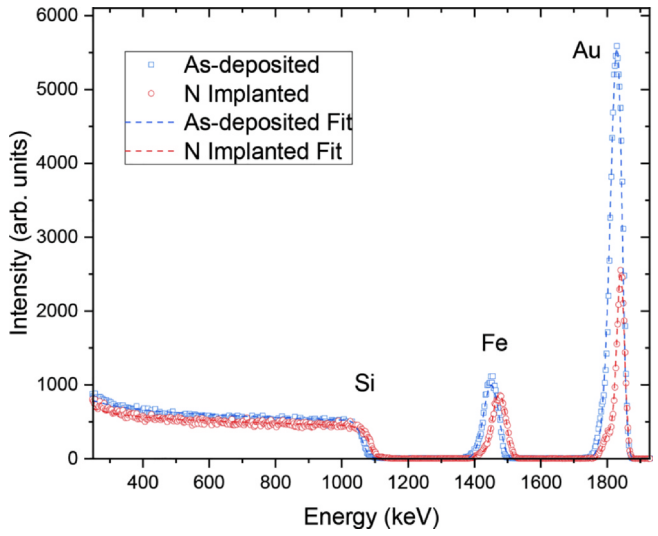

Fig. 2. RBS spectra of as-deposited and implanted films fit with SIMNRA. The fits are represented by dashed lines.

along with their respective fits simulated with SIMNRA. The experimental and fitting error in determination of relative changes in metal concentration in the as-deposited and implanted samples is estimated to be < 1%.

The RBS data is important in understanding and quantifying the compositional changes in the thin film upon N implantation. This is essential for determining the true magnetisation of the implanted film. The RBS spectra record the helium ions backscattered from the thin film. The abscissa denotes the energy of the backscattered particles and the ordinate denotes the number of helium particles backscattered at a specific energy. The spectra of both the as-deposited and implanted films show two peaks. The high energy peak corresponding to gold and low energy peak to iron. The broad plateau observed at even lower energy corresponds to the silicon substrate.

In both samples, Au peak begins at 1846 keV. Considering the incident beam energy and the kinematic factor of gold, the peaks confirm presence of gold at the surface [37,39,40]. However, the onset energy of Fe peak is observed to be higher for the implanted samples and it coincides with the surface scattering energy of iron. This implies that N implantation has bought iron to the surface via. sputtering and intermixing. The SIMNRA fit to the as-deposited RBS spectrum estimates the gold and iron concentration to be 1.47 × 10^{17} cm^{-2} and 3.06 × 10^{17} cm^{-2}, respectively. Assuming the elemental densities for gold and iron, the thicknesses of the Au and Fe layers are estimated to be 25 and 36 nm, respectively. Upon implantation, the gold and iron concentration reduce to 0.59 × 10^{17} cm^{-2} and 2.84 × 10^{17} cm^{-2}, respectively. This denotes a ~8% reduction in iron content upon N implantation. In addition, the elongated Au and Fe tail edge indicate significant intermixing between iron and gold at the surface and iron and silicon at the interface. The results agree with the simulation predictions regarding presence of significant interlayer mixing but we also note that the simulations underestimate the loss in Fe concentration due to implantation induced sputtering effects. This can be expected considering that the T-DYN simulations do not account for density changes, phase transformations and precipitation effects that occur from high fluence implantations [34,36,41].

Estimation of concentration of light elements – N and O from RBS is difficult compared to the heavy elements, especially when the films are deposited on substrate heavier than N and O [40]. Nuclear Reaction Analysis (NRA) was hence performed to measure the N and O concentration in the samples.

Fig. 3 shows the NRA spectrum of the as-deposited and implanted samples. The peak at 9 MeV originates from the nuclear reaction $^{14}N(d,\alpha_0)^{12}C$ and is absent on the as-deposited film [37,39]. Quantifying the peak based on the cross-section for the reaction and with silicon nitride calibration standard as a reference, reveals the nitrogen content of implanted film to be 6.84 ± 0.7 × 10^{16} cm^{-2}. This measured value agrees with the implantation parameters and T-DYN simulations. Oxygen was detected in both the as-deposited and the implanted film (not shown). But the oxygen content has increased upon N implantation. The oxygen in the as-deposited film can be attributed to the native oxide from the silicon substrate. This could lead to partial oxidation of Fe at the Si/Fe interface. The increase in oxygen concentration after implantation can be attributed to the oxidation of the iron exposed at the surface due to the removal of capping layer by sputtering. The oxidation of iron at the surface and at the Si interface could reduce the overall magnetisation of the Fe thin film.

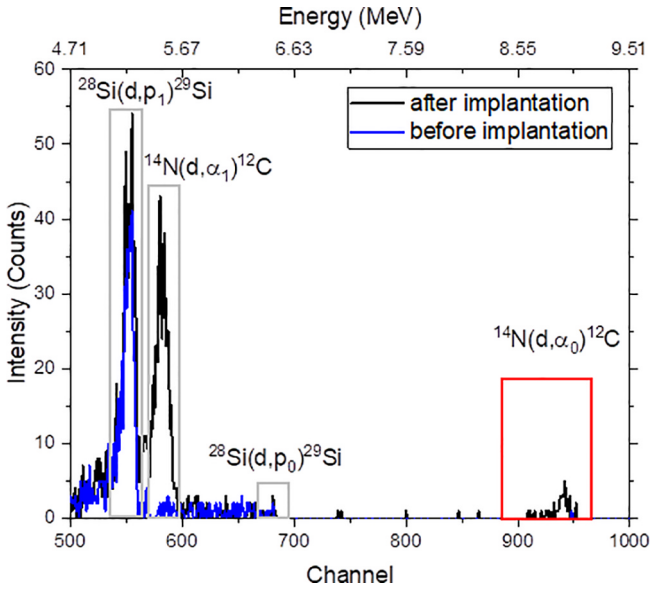

Fig. 3. NRA spectrum of the iron film before and after N implantation. The peak at 9 MeV corresponds to characteristic energy of alpha particles emanating from nuclear reaction $^{14}N(d,\alpha_0)^{12}C$.

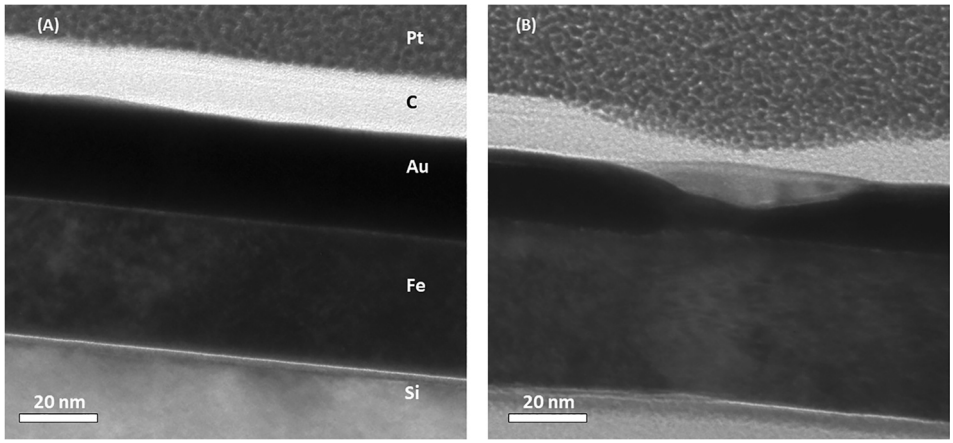

Fig. 4. Cross-sectional TEM image of as-deposited and N implanted Au capped Fe thin film deposited on silicon substrate.

Cross-sectional TEM was performed to analyse the structural and morphological changes caused by N implantation. Fig. 4 shows the cross-sectional TEM image of the as-deposited and implanted thin film samples. The top layers – C and Pt, were deposited during TEM sample preparation to facilitate charge dissipation and sample protection. In the as-deposited sample (Fig. 4A), the different layers composing the sample is clearly visible. Beneath the C layer is the Au capping layer for about 25–27 nm which is followed by Fe layer that extends for 35–37 nm. This is followed by small interfacial Si-Fe layer further followed by crystalline Si substrate. In the implanted sample (Fig. 4B), the surface roughness appears to be significantly enhanced and can be attributed to the sputtering effects induced by implantation. This is supported by atomic force microscopy results, which show that the root-mean-square roughness of the sample increases from < 1 nm to 4 nm upon N implantation. The boundaries of the Au, Fe and Si layers cannot be distinctly determined. The image indicates significant intermixing among the layers as predicted by T-DYN calculations and confirmed by RBS measurements. The intermixing layer at the Si-Fe interface appears to have grown significantly. It is also to be noted that the Si layer immediately following the Fe layer is amorphized due to N implantation. Addition of N atoms into Fe layer is expected to lead to c-axis dilation and reduction in overall density of the Fe layer. However, these changes cannot be accurately quantified due to the concurrent changes induced due to secondary effects of ion implantation (sputtering and intermixing).

High resolution TEM images of the implanted samples were captured to probe their crystal structure. Different lattice orderings are visible from the HR-TEM image shown in Fig. 5. The corresponding Fast Fourier Transform (FFT) of the image is shown in the inset. The FFT image reveals several bright spots positively confirming presence of crystalline order within the implanted film. However, presence of only a small number of bright spots and their weak intensity denote absence of extensive long-range ordering. This is expected from samples prepared by ion beam sputtering and ion implantation at room temperature. Measuring the bright spots in reciprocal space reveals d-spacings of the observed lattice planes to be 0.32 nm, 0.27 nm, 0.21 nm and 0.16 nm (error margin ± 0.01 nm). A d-spacing of 0.32 nm and 0.16 nm is not expected from α-Fe film and could originate from chemically ordered α"-$Fe_{16}N_2$ phase formed by N implantation. Presence of significant volume fraction of α"-$Fe_{16}N_2$ will lead to considerable changes in magnetic properties of the Fe thin films.

The magnetic moment of the samples is measured as a function of applied field using MPMS. Fig. 6 plots the magnetic moment induced in the as-deposited and implanted film against the applied magnetic field. The diamagnetic background from the silicon substrate was subtracted from the measured values. The measurements were carried out with the sample oriented parallel and perpendicular to the applied field.

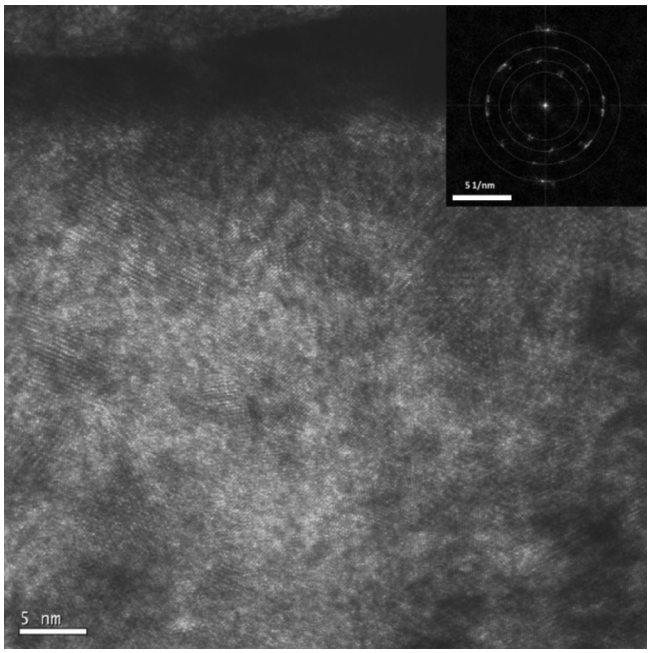

Fig. 5. High Resolution TEM image of N implanted Fe thin film. Inset: Fast Fourier Transform of the implanted TEM image. Bright spots in the Fourier transformed image is fit with dashed circles representing d-spacing of 0.32 nm, 0.27 nm, 0.21 nm and 0.16 nm respectively.

The key focus of this work is to determine the enhancement in magnetic moment of iron film upon N implantation. The saturated moment of the as-deposited iron film was measured to be 738 μemu (both in parallel and perpendicular configuration, as expected) which when normalised against the Fe concentration measured from RBS, equals to 2.09 μ_B/Fe atom. This measured moment is slightly lower than the bulk value (2.2 μ_B/Fe atom) at room temperature. This could possibly be attributed to the formation of non-magnetic iron phases from intermixing of Fe atoms with the Au capping layer at the surface and the native oxide layer of the Si substrate at the interface.

Nitrogen implanted films (blue/green curves) display a markedly different magnetisation behaviour to that of the as-deposited films. The implanted film was measured to have a saturated magnetic moment of 786 μemu. Normalising the implanted film's saturated moment against the Fe concentration obtained for as-deposited film yields a magnetic moment of 2.19 μ_B/Fe atom (green curve). This indicate only a 5% overall enhancement in the magnetisation of nitrogen implanted thin film. However, the Fe concentration of the implanted film reduces by

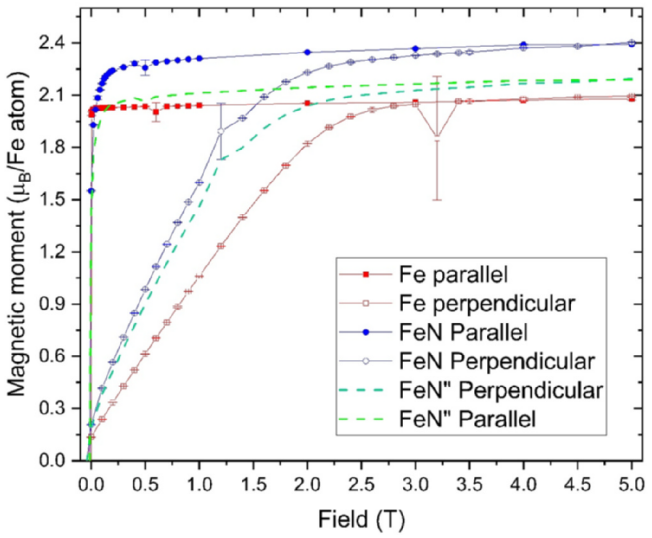

Fig. 6. M/H curve of as-deposited and implanted film in parallel and perpendicular arrangements.

about 8% (refer to RBS discussion) when considering the sputter losses. Recalculating the magnetic moment based on the RBS measurements on the implanted film yields a significantly higher saturated moment of 2.40 μ_B/Fe atom (blue curve). This denotes a 15% enhancement over magnetic moment of unimplanted Fe film. This enhancement is observed despite the reduction in magnetic moment expected from secondary effects of implantation. Thus, it is very likely, that N implantation results in a high volume fraction of α'/α" – $Fe_{16}N_2$ in implanted Fe thin film with large magnetic moments. Fig. 6 (blue and green curves) displays the difference in magnetisation observed with and without consideration of sputter loss due to ion implantation. Observation of such a large difference in the magnetic moments (per Fe atom) of implanted and as-deposited films highlight the importance of considering these effects.

Apart from enhancing the magnetisation, nitrogen implantation is also expected to change the magnetic anisotropy of the thin film considerably. Fe thin films have an in-plane magnetic anisotropy. This can be observed in Fig. 6 (red curves). As-deposited films saturate at < 0.005 T in the parallel orientation. On the perpendicular orientation, an applied magnetic field > 2.8 T is required to achieve saturation. By calculating the area enclosed between the parallel and perpendicular magnetisation curves, the magnetic anisotropy energy (MAE) of the thin films could be determined. Using this method, the MAE of the as-deposited iron film was calculated to be 1.63×10^6 Jm^{-3}. Upon N implantation, the saturation field of the implanted films increases to > 0.02 T in parallel orientation, which is more than four times the saturation field of as-deposited film. On the other hand, in the perpendicular orientation the saturation field reduces to < 2 T. Both these changes indicate a shift towards PMA. The MAE of the implanted film was determined to be 1.34×10^6 Jm^{-3} from the magnetisation curves. This denotes a 18% reduction in MAE in contrast to the 15% rise in the saturated magnetisation upon N implantation.

The magnetic anisotropy of the sample stems from the contributions from magneto-crystalline anisotropy, shape anisotropy and stress-induced anisotropy. Considering that the magneto-crystalline anisotropy of iron is just 4.5×10^4 Jm^{-3} [42], the MAE of the as-deposited films is predominately from the shape anisotropy arising from the demagnetizing energy of the thin film. A rise in saturated magnetisation upon N implantation, will in general increase the area enclosed between the parallel and perpendicular magnetisation curves by an equal proportion. However N implantation reduces the MAE by 2.95×10^5 Jm^{-3}, which suggests that the iron nitride formed by implantation has a perpendicular magnetocrystalline anisotropy that is most likely greater than or equal to -5.4×10^5 Jm^{-3} [43]. However, the PMA induced is still not high enough to overcome the strong demagnetisation effects induced by the thin film geometry (shape anisotropy).

Table 1 summarises results from some of the key works on ferromagnetic iron nitrides synthesized by ion implantation. In all the works, the magnetic moment of iron films was measured before and after implantation. The change in magnetic moment was then normalised against volume fraction of iron nitride formed after implantation to derive the true magnetic moment of iron nitride. As can be observed, the magnetic moment reported for nitrogen implanted iron films range from 2.06 to 2.46 μ_B/Fe. In those works that report the volume fraction of α'/α"-$Fe_{16}N_2$ formed by implantation, the fraction ranges from 21% to 70% respectively. However, the magnetic moment derived for the iron nitride phase is not consistent and ranges from 2.4 to 3.06 μ_B/Fe. It must also be noted, that Amarouche et al. [24] and Garnier et al. [29] for example do not report any enhancement of magnetic moment at all upon N implantation. However, they do report a change in magnetic anisotropy towards perpendicular magnetic anisotropy confirming the formation of nitride phase with elongated c-axis. Such a large disparity in values reported as the magnetic moment of ion beam synthesized iron nitride signify a potential gap in understanding on this subject.

Attempts have been made to explain the wide-ranging values for magnetisation of α'/α"-$Fe_{16}N_2$ by considering the ordering of nitrogen interstitials within the iron lattice [44,45]. However, this is applicable provided that the method used to determine the magnetic moment of nitrogen implanted iron film is accurate. In this work we have shown that large discrepancies may arise if the secondary effects of ion implantation are not accurately measured and considered in magnetic moment calculations. We demonstrated that with and without consideration of sputtering losses, ΔM_s varied from 15% to 5% respectively.

Table 1
Enhancement of magnetic saturation upon N implantation – Comparison against literature. The column **M_s (film)** records the saturated magnetic moment of the N implanted iron film, **ΔM_s** reports the change in overall magnetisation of the sample after implantation, **volume fraction** records the volume fraction of iron nitride in the implanted film and **M_s (α'/α"-$Fe_{16}N_2$)** records the magnetic moment of nitrogen ordered martensite calculated from the volume fraction and M_s (film).

Reference	Energy (keV)	Fluence ($\times 10^{16}$ N cm^{-2})	M_s film (μ_B/Fe)	ΔM_s	Volume fraction	α'/α"-$Fe_{16}N_2$ M_s (μ_B/Fe)
Nakajima et al. [28]	75*	4	2.34**	8%	–	–
		6	2.29**	6%	–	–
		8	2.23**	3%	35%	–
Nakajima et al. [27]	40–130	17.4	–	13.4%	70%	2.66**
Weber at al. [26]	80–230	12.5–16.5 (dose)	2.06	15%	70%	2.47
Shinno et al. [23,25]	50–150	20–140 (dose)	2.3	5%	51%	2.4
Jiang et al. [22]	100	2–50	2.11	12%*	28%	–
			2.26	20%*	21%	–
Amarouche et al [24] Garnier et al [29]	40	10.6	2.17**	0%	–	–
Jiang et al [19] Wang et al [3]	100	50	2.46**	19%	35%	3.06**
This work	32	7 (dose)	2.40	15%	–	–

* Values calculated, not directly stated in original paper **values converted from emu/g or MA/m to μ_B/Fe.

However, we have identified from the literature review that most of the works on ion beam synthesized iron nitrides ignore the influence of sputtering effects caused by implantation on the magnetisation of implanted thin films [3,19,22–25,28,29]. It is interesting to note that [24,29] do report the loss of the protective capping layer (gold) from sputtering upon implantation similar to this work. However, they have not directly measured the iron concentration after implantation to rule out any significant sputter losses. Measurement of changes in thicknesses of the sample with implantation cannot substitute direct measurement of iron concentration using methods such as RBS. This is because high fluence implantation is also expected to cause density changes, lattice dilation and phase transformation in addition to other secondary effects such as interlayer mixing, and partial oxidation of iron exposed to the surface [41].

To the best of our knowledge, only two studies considered the secondary effects of ion implantation in determining the magnetic moment of iron nitrides [26,27]. Nakajima et al [27] reported a 9% increase in saturated magnetisation after N implantation. After considering the sputter losses this enhancement was revised to 13.4%. It must however be noted that the sputter losses in this work was not directly determined but rather was based on extrapolation of values from previous work which were not performed in the same parameter range. Weber et al. [26] on the other hand directly measured the Fe concentration before and after implantation using RBS and normalised the change in magnetisation accordingly. He further considered the loss in magnetic moment due to intermixing between Au and Fe layers and reported the overall enhancement in magnetisation to be 15% which agrees with our reported values. This strongly suggests that consistent results can be obtained by carefully considering the secondary effects of ion implantation in determining the magnetic moment of the implanted samples.

4. Conclusion

We have implanted ion beam sputtered Fe thin film covered with an Au capping layer with a dose of 7×10^{16} N/cm^2. T-DYN simulations predicts the average N concentration to be 13 at.% in the iron layers with significant sputtering losses from implantation. Ion beam analysis shows that the effective iron concentration in the sample reduces by 8% upon implantation with significant concentration of iron reaching the surface. Ion implantation also leads to significant intermixing between iron and gold at the surface and iron and silicon at the interface. Cross-sectional TEM and AFM also reveal sputtering induced roughening of the sample surface. Magnetic measurements, however, show that despite the secondary effects of ion implantation, the saturated magnetic moment of the overall film increases from 2.09 to 2.4 μ_B/Fe suggesting a significant volume of α-Fe to have converted to α"-$Fe_{16}N_2$. HR-TEM imaging of the implanted sample and their corresponding FFT analysis support these findings. The nitride formation also results in significant reduction in in-plane magnetic anisotropy. This can possibly be attributed to the perpendicular magnetocrystalline anisotropy reported for α"-$Fe_{16}N_2$. Comparison against literature shows the importance of considering the secondary effects of implantation – sputtering losses and surface recession in determining the magnetic moment of implanted films. In this work we demonstrate that with and without consideration of these effects, the enhancement in saturated moment decreases from 15% to 5%. Therefore, it is necessary to measure and account for the secondary effects of ion implantation in magnetic moment calculations to obtain consistent magnetisation values for ion beam synthesized iron nitrides.

5. Prime novelty statement

- Nitrogen incorporation into the interstitial sites of iron leads to formation of iron nitrides with applications in diverse fields such as catalysis, cancer treatment, lightweight permanent magnets, electrochemical energy devices, corrosion and wear-resistant surfaces.
- Nitrogen implantation significantly reduces the in-plane magnetic anisotropy of the sample due to formation of α"-$Fe_{16}N_2$ with perpendicular magnetic anisotropy.
- Measurement and consideration of sputter losses from N implantation is demonstrated to be crucial in determining the magnetisation of N implanted iron thin films accurately.
- Review of literature shows lack of proper accounting for secondary effects of ion implantation leading to reporting of inconsistent and reduced magnetic moments for ion beam synthesized α"-$Fe_{16}N_2$.

CRediT authorship contribution statement

P. Gupta: Conceptualization, Methodology, Data curation, Investigation, Formal analysis, Writing - original draft, Supervision, Visualization. **H. Fiedler:** Methodology, Data curation, Investigation, Formal analysis. **S. Rubanov:** Data curation, Formal analysis. **J. Kennedy:** Supervision, Validation, Project administration.

Declaration of Competing Interest

The authors declare that they have no known competing financial interests or personal relationships that could have appeared to influence the work reported in this paper.

Acknowledgement

The authors would like to thank Dr Simon Granville from Robinson Research Institute for his valuable feedback on this work and Mr Chris Purcell from GNS Science for his assistance in carrying out the ion beam analysis work. This research is funded by the Ministry of Business, Innovation and Employment, New Zealand under the research contract RTVU1811 and the MacDiarmid Institute for Advanced Materials and Nanotechnology, funded by the New Zealand Centres of Excellence Fund.

References

[1] H. Yin, C. Zhang, F. Liu, Y. Hou, Hybrid of iron nitride and nitrogen-doped graphene aerogel as synergistic catalyst for oxygen reduction reaction, Adv. Funct. Mater. 24 (20) (2014) 2930–2937.
[2] M. Shibata, T. Ogawa, M. Kawashita, Synthesis of iron nitride nanoparticles from magnetite nanoparticles of different sizes for application to magnetic hyperthermia, Ceram. Int. 45 (17) (2019) 23707–23714.
[3] J.-P. Wang, Environment-friendly bulk Fe16N2 permanent magnet: Review and prospective, J. Magn. Magn. Mater. 497 (2020) 165962.
[4] Wang, J.-P.; He, S.; Jiang, Y. 2018. Iron nitride permanent magnet and technique for forming iron nitride permanent magnet. U.S. Patent No. 10,068,689.
[5] J.L. Rowsell, V. Pralong, L.F. Nazar, Layered lithium iron nitride: a promising anode material for Li-ion batteries, J. Am. Chem. Soc. 123 (35) (2001) 8598–8599.
[6] Y. Wang, C. Xie, D. Liu, X. Huang, J. Huo, S. Wang, Nanoparticle-stacked porous nickel–iron nitride nanosheet: A highly efficient bifunctional electrocatalyst for overall water splitting, ACS Appl. Mater. Interfaces 8 (29) (2016) 18652–18657.
[7] T. Weber, L. De Wit, F. Saris, A. Königer, B. Rauschenbach, G. Wolf, S. Krauss, Hardness and corrosion resistance of single-phase nitride and carbide on iron, Mater. Sci. Eng., A 199 (2) (1995) 205–210.
[8] Inoue, T.; Sasaki, Y. 2010. Iron nitride magnetic powder and magnetic recording medium comprising the same. U.S. Patent No. 12/534,998.
[9] Sankar, S.G.; Simizu, S.; Zande, B.J.; Obermyer, R.T. 2013. Iron nitride powders for use in magnetic, electromagnetic, and microelectronic devices. U.S. Patent No. 8, 535,634.
[10] D. Borsa, S. Grachev, J. Kerssemakers, D. Boerma, Development of an all-nitride magnetic tunnel junction, J. Magn. Magn. Mater. 240 (1–3) (2002) 445–447.
[11] A. Narahara, K. Ito, T. Suemasu, Growth of ferromagnetic Fe4N epitaxial layers and a-axis-oriented Fe4N/MgO/Fe magnetic tunnel junction on MgO (0 0 1) substrates using molecular beam epitaxy, J. Cryst. Growth 311 (6) (2009) 1616–1619.
[12] J. Coey, P. Smith, Magnetic nitrides, J. Magn. Magn. Mater. 200 (1–3) (1999) 405–424.
[13] L. You, R. Sousa, S. Bandiera, B. Rodmacq, B. Dieny, Co/Ni multilayers with perpendicular anisotropy for spintronic device applications, Appl. Phys. Lett. 100 (17) (2012) 172411.
[14] B. Tudu, A. Tiwari, Recent developments in perpendicular magnetic anisotropy thin

films for data storage applications, Vacuum 146 (2017) 329–341.
[15] N. Ji, X. Liu, J. Wang, Theory of giant saturation magnetization in α ″-Fe16N2: role of partial localization in ferromagnetism of 3d transition metals, New J. Phys. 12 (6) (2010) 063032.
[16] Y. Sugita, K. Mitsuoka, M. Komuro, H. Hoshiya, Y. Kozono, M. Hanazono, Giant magnetic moment and other magnetic properties of epitaxially grown Fe16N2 single-crystal films, J. Appl. Phys. 70 (10) (1991) 5977–5982.
[17] M. Takahashi, H. Shoji, α″-Fe16N2 problem—giant magnetic moment or not, J. Magn. Magn. Mater. 208 (3) (2000) 145–157.
[18] M. Takahashi, H. Shoji, H. Takahashi, H. Nashi, T. Wakiyama, M. Doi, M. Matsui, Magnetic moment of α″-Fe16N2 films, J. Appl. Phys. 76 (10) (1994) 6642–6647.
[19] Y. Jiang, M. Al Mehedi, E. Fu, Y. Wang, L.F. Allard, J.-P. Wang, Synthesis of Fe 16 N 2 compound free-standing foils with 20 MGOe magnetic energy product by nitrogen ion-implantation, Sci. Rep. 6 (2016) 25436.
[20] T. Kim, M. Takahashi, New magnetic material having ultrahigh magnetic moment, Appl. Phys. Lett. 20 (12) (1972) 492–494.
[21] S. Bhattacharyya, Iron nitride family at reduced dimensions: a review of their synthesis protocols and structural and magnetic properties, J. Phys. Chem. C 119 (4) (2015) 1601–1622.
[22] Y. Jiang, M. Al Mehedi, E. Fu, Y. Wang, J.-P. Wang, FeN foils by nitrogen ion-implantation, J. Appl. Phys. 115 (17) (2014) 17A753.
[23] H. Shinno, M. Uehara, K. Saito, Synthesis of α ″-Fe16N2 iron nitride by means of nitrogen-ion implantation into iron thin films, J. Mater. Sci. 32 (9) (1997) 2255–2261.
[24] T. Amarouche, L.-C. Garnier, M. Marangolo, M. Eddrief, V. Etgens, F. Fortuna, Y. Sadaoui, M. Tamine, J. Cantin, H. Von Bardeleben, Influence of ion implantation parameters on the perpendicular magnetic anisotropy of Fe-N thin films with stripe domains, J. Appl. Phys. 121 (24) (2017) 243903.
[25] H. Shinno, K. Saito, Effects of film thickness on formation processes of Fe16N2 in nitrogen ion-implanted Fe films, Surf. Coat. Technol. 103 (1998) 129–134.
[26] T. Weber, L. De Wit, F. Saris, P. Schaaf, Search for giant magnetic moments in ion-beam-synthesized α″-Fe16N2, Thin Solid Films 279 (1–2) (1996) 216–220.
[27] K. Nakajima, S. Okamoto, Large magnetization induced in single crystalline iron films by high-dose nitrogen implantation, Appl. Phys. Lett. 56 (1) (1990) 92–94.
[28] K. Nakajima, S. Okamoto, T. Okada, Formation of ferromagnetic iron nitrides in iron thin films by high-dose nitrogen ion implantation, J. Appl. Phys. 65 (11) (1989) 4357–4361.
[29] L.-C. Garnier, M. Eddrief, S. Fin, D. Bisero, F. Fortuna, V. Etgens, M. Marangolo, Perpendicular magnetic anisotropy in Fe–N thin films: threshold field for irreversible magnetic stripe domain rotation, Spin. World Sci. 6 (04) (2016) 1640014.
[30] J. Jagielski, M. Kopcewicz, G. Gawlik, W. Matz, L. Thome, Thickness dependent phase transformations in implanted iron layers, J. Appl. Phys. 91 (10) (2002) 6465–6470.
[31] A. Mahendra, P. Gupta, P.P. Murmu, W.J. Trompetter, J. Kennedy, Fabrication of superparamagnetic permalloy nanostructures in ZnO matrix by ion beam sputtering, Mater. Today:. Proc. (2020), https://doi.org/10.1016/j.matpr.2020.05.475.
[32] H. Fiedler, P. Gupta, J. Kennedy, A. Markwitz, 28Si+ ion beams from Penning ion source based implanter systems for near-surface isotopic purification of silicon, Rev. Sci. Instrum. 89 (12) (2018) 123305.
[33] A. Markwitz, J. Kennedy, Group-IV and V ion implantation into nanomaterials and elemental analysis on the nanometre scale, Int. J. Nanotechnol. 6 (3–4) (2009) 369–383.
[34] J. Biersack, TRIM-DYNAMIC applied to marker broadening and SIMS depth profiling, Nucl. Instrum. Methods Phys. Res., Sect. B 153 (1–4) (1999) 398–409.
[35] W. Eckstein, J. Biersack, Computer simulation of two-component target sputtering, Appl. Phys. A 37 (2) (1985) 95–108.
[36] W. Möller, W. Eckstein, J. Biersack, Tridyn-binary collision simulation of atomic collisions and dynamic composition changes in solids, Comput. Phys. Commun. 51 (3) (1988) 355–368.
[37] J. Kennedy, A. Markwitz, H. Trodahl, B. Ruck, S. Durbin, W. Gao, Ion beam analysis of amorphous and nanocrystalline group III-V nitride and ZnO thin films, J. Electron. Mater. 36 (4) (2007) 472–482.
[38] L.A. Giannuzzi, J.L. Drown, S.R. Brown, R.B. Irwin, F.A. Stevie, Applications of the FIB lift-out technique for TEM specimen preparation, Microsc. Res. Tech. 41 (4) (1998) 285–290.
[39] M. Mayer, SIMNRA, a simulation program for the analysis of NRA, RBS and ERDA, AIP Conference Proceedings, American Institute of Physics, 1999, pp. 541–544.
[40] W.-K. Chu, Backscattering Spectrometry, Elsevier, 2012.
[41] P. Gupta, Structural and Magnetic Properties of Cobalt Implanted Diamond-like Carbon Films Synthesized by Ion Beam Methods Doctoral Dissertation, Victoria University of Wellington, 2017.
[42] B.D. Cullity, C.D. Graham, Introduction to Magnetic Materials, John Wiley & Sons, 2011.
[43] H. Takahashi, M. Igarashi, A. Kaneko, H. Miyajima, Y. Sugita, Perpendicular uniaxial magnetic anisotropy of Fe16N2 [001] single crystal films grown by molecular beam epitaxy, IEEE Trans. Magn. 35 (5) (1999) 2982–2984.
[44] N. Ji, L.F. Allard, E. Lara-Curzio, J.-P. Wang, N site ordering effect on partially ordered Fe16N2, Appl. Phys. Lett. 98 (9) (2011) 092506.
[45] J.-P. Wang, N. Ji, X. Liu, Y. Xu, C. Sanchez-Hanke, Y. Wu, F. De Groot, L.F. Allard, E. Lara-Curzio, Fabrication of Fe16N2 films by sputtering process and experimental investigation of origin of giant saturation magnetization in Fe16N2, IEEE Trans. Magn. 48 (5) (2012) 1710–1717.